NAVIGATION: *Journal of The Institute of Navigation*
Vol. 35, No. 4, Winter 1988–89
Printed in U.S.A.

Navigation System Integrity Monitoring Using Redundant Measurements

MARK A. STURZA

Litton Systems, Inc., Woodland Hills, California
Received January 1988
Revised October 1988

ABSTRACT

The advantages of a navigation system that can monitor its own integrity are obvious. Integrity monitoring requires that the navigation system detect faulty measurement sources before they corrupt the outputs. This paper describes a parity approach to measurement error detection when redundant measurements are available. The general form of the detector operating characteristic (DOC) is developed. This equation relates the probability of missed detection to the probability of false alarm, the measurement observation matrix, and the ratio of the detectable bias shift to the standard deviation of the measurement noise.

Two applications are presented: skewed axis strapdown inertial navigation systems, where DOCs are used to compare the integrity monitoring capabilities of various redundant sensor strapdown system configurations; and GPS navigation sets, where DOCs are used to discuss GPS integrity monitoring for meeting nonprecision approach requirements. A fault identification algorithm is also presented.

INTRODUCTION

The Federal Radionavigation Plan [1] defines navigation system integrity monitoring as "the ability of a system to provide timely warnings to users when the system should not be used for navigation." To implement integrity monitoring, the navigation system must detect faulty measurement sources before they result in out-of-specification performance. This in turn requires measurement redundancy. One redundant measurement is necessary for detecting a faulty measurement source. If additional redundant measurements are available, it is possible to isolate the faulty measurement source.

Integrity monitoring can be applied to any navigation system that provides redundant measurements. Potential applications include skewed axis strapdown inertial navigation systems (INSs), GPS, Omega, and Loran-C. The INS and GPS applications will be used as examples to illustrate the theory.

Conventional INSs are configured with three gyro/accelerometer pairs mounted on orthogonal axes. Integrity monitoring can be achieved externally only by comparing the outputs of two or more such systems. A single redundant sensor INS incorporating four or more sensor pairs can provide internal integrity monitoring. The benefits of one redundant sensor INS versus two or more

conventional INSs are significant. Typical redundant sensor INSs incorporate four, five, or six pairs of inertial sensors [2, 3, 4, 5, 6, 7, 8].

Conventional GPS navigation requires measurements from 4 satellites to resolve three spatial dimensions and time. With the baseline 18-satellite constellation, 5 or more satellites will be available 99.3 percent of the time. By using the redundant measurement(s), it is possible to provide integrity monitoring. This is a requirement if GPS is to be certified as a sole means navigation system [1]. If measurements from 6 or more satellites are available, it is possible to isolate the faulty satellite and continue operating with the remaining ones. Considerable interest in GPS self-integrity monitoring has been sparked by the activities of the Radio Technical Commission for Aeronautics Special Committee-159 Integrity Working Group [9, 10].

The theory for both inertial navigation and radionavigation integrity monitoring is the same. This theory will be developed in the next three sections.

MEASUREMENT MODEL

The general case of M measurements in an N dimensional state space, $M \geq N + 1$, is addressed. The measurement equation is:

$$\mathbf{z} = \mathbf{H}\mathbf{x} + \mathbf{n} + \mathbf{b} \tag{1}$$

where $\mathbf{z}$ is the $M \times 1$ vector of measurements compensated with all a priori information; $\mathbf{H}$ is the $M \times N$ measurement matrix which transforms from the state space to the measurement space, rank $[\mathbf{H}] = N$; $\mathbf{x}$ is the $N \times 1$ state vector; $\mathbf{n}$ is the $M \times 1$ vector of Gaussian measurement noise, $E[\mathbf{n}] = \mathbf{0}$ and $COV[\mathbf{n}] = \sigma_n^2 \mathbf{I}_M$, where $\mathbf{I}_M$ is the identity matrix of order M; and $\mathbf{b}$ is the $M \times 1$ vector of uncompensated measurement biases (faults).

The fault model is a single measurement source failure resulting in a step bias shift. A failure of measurement source i is modeled by $\mathbf{b} = \mathbf{b}_i$, where $\mathbf{b}_i$ is an $M \times 1$ vector with ith element B and zeros elsewhere. If there are no faults, then $\mathbf{b} = \mathbf{0}$.

In the INS application, the gyro and accelerometer measurements are considered separately. In both cases, $N = 3$ and $M \geq 4$. The measurement vector, $\mathbf{z}$, contains the $\Delta\theta$s (gyro measurements) or ΔVs (accelerometer measurements) compensated for scale factor and biases. The state vector, $\mathbf{x}$, consists of the three orthogonal body $\Delta\theta$s or ΔVs. The measurement matrix, $\mathbf{H}$, consists of the unit projection vectors from the sensor axis to the orthogonal body axis. It is assumed that $\mathbf{H}$ is known perfectly (there are no uncompensated misalignments).

In the GPS application, the pseudorange residual ($\widetilde{PR}$) and delta-range residual ($\widetilde{\Delta R}$) measurements are considered separately. For both types of measurements, $N = 4$ and $M \geq 5$. The measurement vector, $\mathbf{z}$, contains the $\widetilde{PR}$ measurements or the $\widetilde{\Delta R}$ measurements compensated for atmospheric effects and clock biases. The state vector, $\mathbf{x}$, consists of three orthogonal positions and clock bias for the $\widetilde{PR}$ measurements, or three orthogonal velocities and clock bias rate for the $\widetilde{\Delta R}$ measurements. The $\widetilde{PR}$ measurement matrix consists of the line-of-sight (LOS) vectors to the satellites, with 1s in the fourth column corresponding to the clock bias state. The $\widetilde{\Delta R}$ measurement matrix consists of the LOS vectors to the satellites, with ΔTs in the fourth column corresponding to the

clock bias rate state, where ΔT is the delta-range interval. It is again assumed that **H** is known perfectly.

PARITY VECTOR

In this section, an $(M - N) \times 1$ parity vector, **p**, is constructed. It is shown that:

1) **p** is independent of the state vector **x**.
2) If there is no fault, $\mathbf{b} = \mathbf{0}$, then $E[\mathbf{p}] = \mathbf{0}$.
3) If there is a fault, $\mathbf{b} = \mathbf{b}_i$ for some i, then $E[\mathbf{p}]$ is a function of B.

Thus **p** can be used for fault detection. An $M \times 1$ fault vector, **f**, is constructed by transforming **p** to the measurement space.

The least squares estimate of the state vector in equation (1) is

$$\begin{aligned} \hat{\mathbf{x}} &= \mathbf{H}^*\mathbf{z} \\ &= \mathbf{x} + \mathbf{H}^*(\mathbf{n} + \mathbf{b}) \end{aligned} \tag{2}$$

where $\mathbf{H}^* = (\mathbf{H}^T\mathbf{H})^{-1}\mathbf{H}^T$ is the $N \times M$ generalized inverse of **H**. The matrix $\mathbf{H}^*$ represents a transformation from the measurement space to the state space.

For a given $M \times N$ measurement matrix **H** with rank N, it is possible to find an $(M - N) \times M$ matrix **P** such that rank $[\mathbf{P}] = M - N$, $\mathbf{PP}^T = \mathbf{I}_M$, and $\mathbf{PH} = 0$. The matrix **P** spans the null space of **H** (the parity space). The rows of **P** are orthogonal unit basis vectors for the parity space.

The $M \times M$ matrix

$$\mathbf{A} = \begin{bmatrix} \mathbf{H}^* \\ \cdots\cdots \\ \mathbf{P} \end{bmatrix}$$

has rank M. The linear transformation represented by **A** separates the M dimensional measurement space into two subspaces: an N dimensional state space and an $M - N$ dimensional parity space

$$\begin{bmatrix} \text{state space} \\ \cdots\cdots\cdots \\ \text{parity space} \end{bmatrix} = \mathbf{A} \begin{bmatrix} \text{measurement} \\ \text{space} \end{bmatrix}$$

The $(M - N) \times 1$ parity vector given by

$$\begin{aligned} \mathbf{p} &= \mathbf{Pz} \\ &= \mathbf{P}(\mathbf{n} + \mathbf{b}) \end{aligned} \tag{3}$$

is independent of **x** since $\mathbf{PH} = 0$ (if **H** is not exact, then the parity vector is no longer independent of the state). The elements of **p** are jointly normally distributed, characterized by their expected value and covariance:

$$E[\mathbf{p}] = \mathbf{Pb}$$

and

$$\text{COV}[\mathbf{p}] = \sigma_n^2 \mathbf{I}_{M-N}.$$

Thus the elements of **p** are uncorrelated with equal variance, the same variance as the measurement noise. If there is no fault, **b** = **0**, then E[**p**] = 0.

The M × M matrix

$$\mathbf{A}^{-1} = [\mathbf{H}|\mathbf{P}^T]$$

has rank M and represents the inverse transformation represented by A. It transforms from the state space and the parity space to the measurement space:

$$\begin{bmatrix} \text{measurement} \\ \text{space} \end{bmatrix} = \mathbf{A}^{-1} \begin{bmatrix} \text{state space} \\ \cdots\cdots\cdots \\ \text{parity space} \end{bmatrix}$$

Thus the transformation of the parity vector to the measurement space is given by

$$\begin{aligned} \mathbf{f} &= [\mathbf{H}|\mathbf{P}^T] \begin{bmatrix} \mathbf{0} \\ \mathbf{p} \end{bmatrix} \\ &= \mathbf{Sz} \end{aligned} \tag{4}$$

where $\mathbf{S} = \mathbf{P}^T\mathbf{P}$ is an M × M matrix. The matrix S has rank M − N and is idempotent ($\mathbf{S}^2 = \mathbf{S}$). The M × 1 fault vector, **f**, is characterized by:

$$E[\mathbf{f}] = \mathbf{Sb}$$

and

$$COV[\mathbf{f}] = \sigma_n^2\mathbf{S}.$$

The S matrix can be directly calculated from **H**:

$$\mathbf{S} = \mathbf{I}_M - \mathbf{H}\mathbf{H}^*$$

This equation is derived in Appendix A.

FAULT DETECTION

Fault detection is based on hypothesis testing. A decision variable, D, is constructed and tested against a threshold, T. The hypothesis test is

$$D \underset{H_0}{\overset{H_1}{\gtrless}} T$$

where H_0 is the null hypothesis (no fault, **b** = **0**), and H_1 is the fault hypothesis (**b** = $\mathbf{b}_i$ for some i). Thus if D>T, a fault is detected; otherwise no fault is detected. The performance of the test is characterized by the probability of false alarm (P_{FA}) and the probability of missed detection (P_{MD}):

$$\begin{aligned} P_{FA} &= P\,[D>T|H_0] \\ P_{MD} &= P\,[D<T|H_1]. \end{aligned}$$

The detector operating characteristics (DOCs) are obtained by plotting P_{MD} vs P_{FA} for various combinations of parameters.

The decision variable considered is the square of the magnitude of the parity vector, which is equivalent to the quadratic form $D = \mathbf{p}^T\mathbf{p}$. It is equal to the square of the magnitude of the fault vector, $D = \mathbf{f}^T\mathbf{f}$. This decision variable is popular in the literature [7, 11].

The hypothesis test is characterized by

$$P_{FA} = P\,[D>T|\mathbf{b} = \mathbf{0}]$$

and, assuming that measurement faults are equally likely,

$$P_{MD} = \frac{1}{M}\sum_{i=1}^{M} P\,[D<T|\mathbf{b}=\mathbf{b}_i].$$

If $\mathbf{b} = \mathbf{0}$, then $E[\mathbf{p}] = \mathbf{0}$, and D/σ_n^2 has chi-square distribution with $M - N$ degrees of freedom. Thus

$$P_{FA} = Q\,(T/\sigma_n^2|M - N) \tag{5}$$

where $Q(\chi^2|r) = 1 - P(\chi^2|r)$, and $P(\chi^2|r)$ is the chi-square probability function

$$P(\chi^2|r) = \left[2^{r/2}\,\Gamma\left(\frac{r}{2}\right)\right]^{-1}\int_0^{\chi^2} t^{r/2-1}\,e^{-t/2}\,dt. \tag{6}$$

P_{FA} depends on $M - N$, the number of redundant measurements, and is otherwise independent of H. For given P_{FA}, $M - N$, and σ_n^2, the required threshold is given by

$$T\,(P_{FA}, M - N, \sigma_n^2) = \sigma_n^2\,Q^{-1}\,(P_{FA}|M - N) \tag{7}$$

where $Q^{-1}(P|r)$ is the inverse function of $Q(\chi^2|r)$. Values of the threshold-to-noise variance ratio, T/σ_n^2, as a function of P_{FA} are shown in Table 1 for one, two, and three redundant measurements.

If $\mathbf{b} = \mathbf{b}_i$, then $E[\mathbf{p}] = \mathbf{P}\mathbf{b}_i$, and D/σ_n^2 has noncentral chi-square distribution with $M - N$ degrees of freedom and noncentrality parameter

$$\theta_i = \left(B^2/\sigma_n^2\right) S_{ii}$$

Table 1—Threshold-to-Noise Variance Ratio (T/σ_n^2)

	Number of Redundant Measurements (M – N)		
P_{FA}	1	2	3
10^{-1}	2.71	4.61	6.25
10^{-2}	6.63	9.21	11.34
10^{-3}	10.83	13.82	16.27
10^{-4}	15.14	18.42	21.11
10^{-5}	19.51	23.03	25.90
10^{-6}	23.93	27.63	30.66
10^{-7}	28.37	32.24	35.41
10^{-8}	32.84	36.84	40.13
10^{-9}	37.32	41.45	44.84

where S_{ii} is the ith diagonal element of **S**. Thus

$$P_{MD} = \frac{1}{M} \sum_{i=1}^{M} P\left(T/\sigma_n^2 \mid M - N, \frac{B^2}{\sigma_n^2} S_{ii}\right) \tag{8}$$

where $P(\chi^2|r, \theta)$ is the noncentral chi-square probability function

$$P(\chi^2|r, \theta) = \sum_{j=0}^{\infty} e^{-\theta/2} \frac{(\theta/2)^j}{j!} P(\chi^2|r+2j). \tag{9}$$

The DOC is given by

$$P_{MD}\left(P_{FA}, M - N, \{S_{ii}\}, \frac{B}{\sigma_n}\right)$$

$$= \frac{1}{M} \sum_{i=1}^{M} P\left(Q^{-1}(P_{FA}|M - N)|M - N, \frac{B^2}{\sigma_n^2} S_{ii}\right) \tag{10}$$

P_{MD} depends on the ratio B/σ_n and not on the individual values. Calculation of the DOC is discussed in Appendix B.

To summarize, the fault detection algorithm is as follows:

1) Based on the required P_{FA}, the number of redundant measurements, $M - N$, and the measurement noise variance, σ_n^2, calculate the threshold

$$T = \sigma_n^2 Q^{-1}(P_{FA}|M - N).$$

2) Calculate the fault vector, $\mathbf{f} = \mathbf{Sz}$.
3) Calculate the decision variable, $D = \mathbf{f}^T\mathbf{f}$.
4) If $D > T$, then declare that a fault has occurred.
5) Repeat steps 2, 3, and 4 for each new measurement vector.

INTEGRITY MONITORING PERFORMANCE

Inertial Navigation System

Two general M sensor skewed axis inertial sensor geometries are considered. The first is M sensors equally spaced on a cone with half-angle α. For $M = 4$ and $\alpha = 54.736$ deg, this is the octahedral tetrad [2, 3]. For $M = 6$ and $\alpha = 54.736$ deg, this is the skewed triad hexad [2, 4]. The skewed triad hexad geometry is also obtained by mounting two triads, one inverted apex to apex, with a 60 deg skew. Another way to achieve the skewed triad geometry is to mount two triads in close proximity, one skewed 60 deg to the other. The equivalent skewed triad configurations are shown in Figure 1.

The S matrix for M sensors equally spaced on a cone is independent of the cone half-angle, α. The diagonal elements are equal, given by

$$S_{ii} = \frac{M-3}{M}.$$

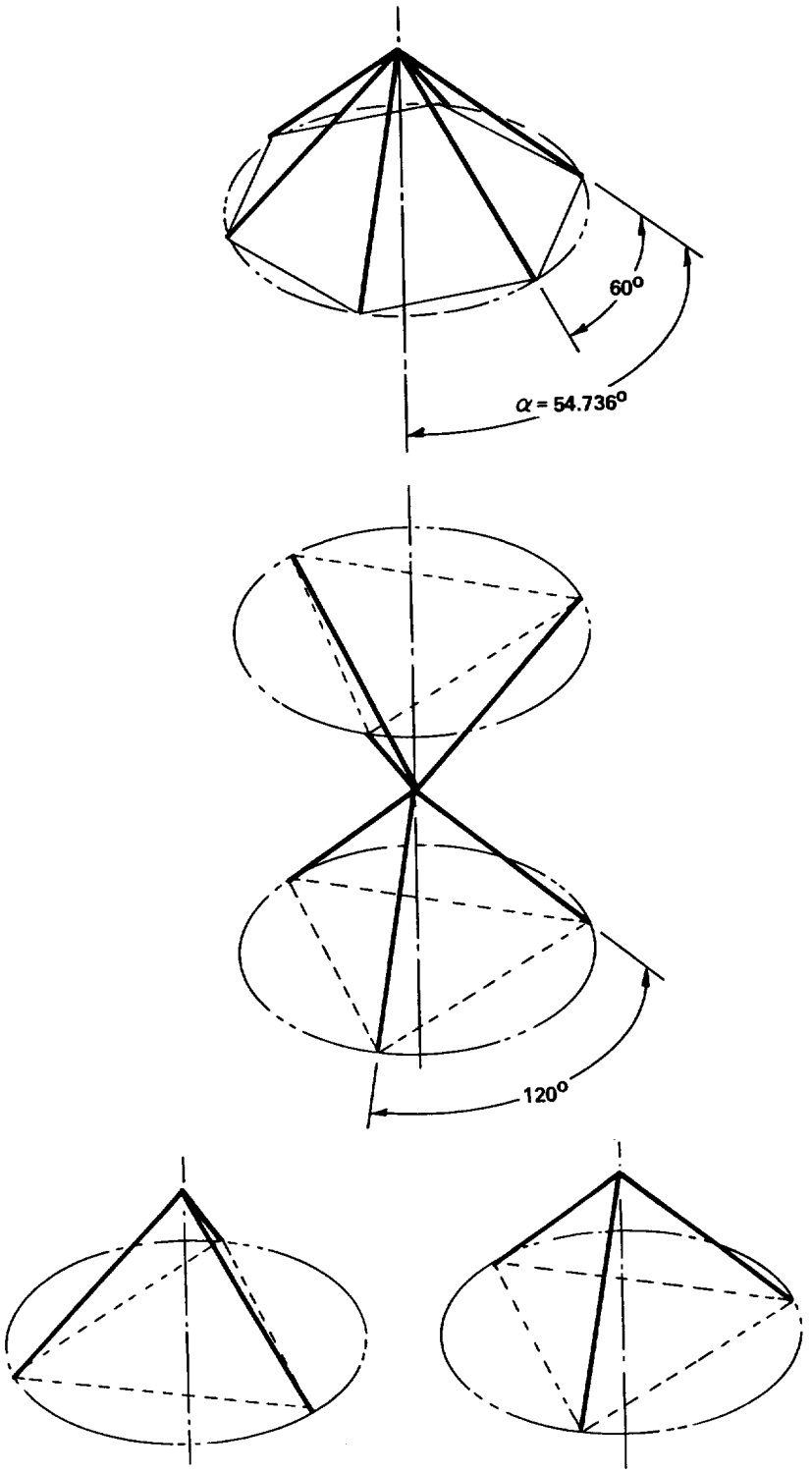

Fig. 1—Equivalent Skewed Triad Configurations

The values of S_{ii} as a function of M are as follows:

Number of Sensors (M)	S_{ii}
4	0.25
5	0.40
6	0.50

The second M sensor geometry considered is M – 1 sensors equally spaced on a cone, with half-angle α and one sensor on the cone axis. For M = 4 and α = 70.529 deg, this is the tetrahedral tetrad [5]. For M = 4 and α = 54.736 deg, this is the three orthogonal and one on the diagonal tetrad [6]. For M = 6 and α = 63.435 deg, this is the dodecahedral hexad [2, 5, 7].

The S matrix diagonal elements for the M – 1 sensors equally spaced on a cone and one sensor on the cone axis are as follows:

$$S_{11} = \frac{M \cos^2 \alpha}{1 + M \cos^2 \alpha}$$

$$S_{ii} = 1 - \frac{2}{M} - \frac{\cos^2 \alpha}{1 + M \cos^2 \alpha} \quad i = 2,..., M$$

The cone half-angles required to achieve equal fault detection performance for all M sensors are as follows:

Number of Sensors (M)	α ($S_{11} = S_{ii}$)	S_{ii}
4	70.529°	0.25
5	65.905°	0.40
6	63.435°	0.50

These configurations are seen to provide the same fault detection performance as the configurations with M sensors equally spaced on a cone. The S matrix diagonal elements for the three orthogonal and one on the diagonal tetrad are:

$$S_{11} = 0.5$$

$$S_{ii} = 0.167 \qquad i = 2, 3, 4.$$

DOCs for the configurations of four, five, and six sensors on a cone for various B/σ_n ratios are shown in Figures 2, 3, and 4, respectively. Figure 5 compares DOCs for the three configurations for B/σ_n = 15. As expected, the performance improves as the number of sensors increases. Figure 6 compares the DOCs for the configurations of four sensors on a cone, and three orthogonal and one on the diagonal. The configuration of four sensors on a cone provides significantly superior fault detection capability.

Consider INSs with four, five, and six sensors equally spaced on a cone, constructed from gyros with white noise W_G = 0.00015 deg/$\sqrt{\text{hr}}$ and accelerometers with white noise W_A = 70 μg/$\sqrt{\text{Hz}}$. Define a fault as a step bias shift resulting in a peak Schuler velocity of 5 kn (8.4 ft/s). The short-term Schuler velocity error propagation equations for a step bias shift are:

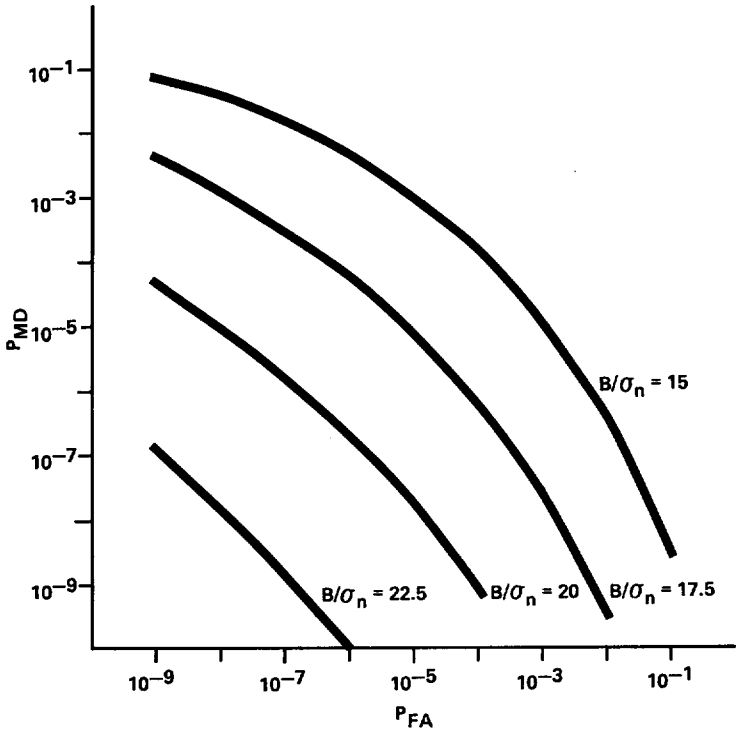

Fig. 2—DOCs for Four Sensors Equally Spaced on a Cone

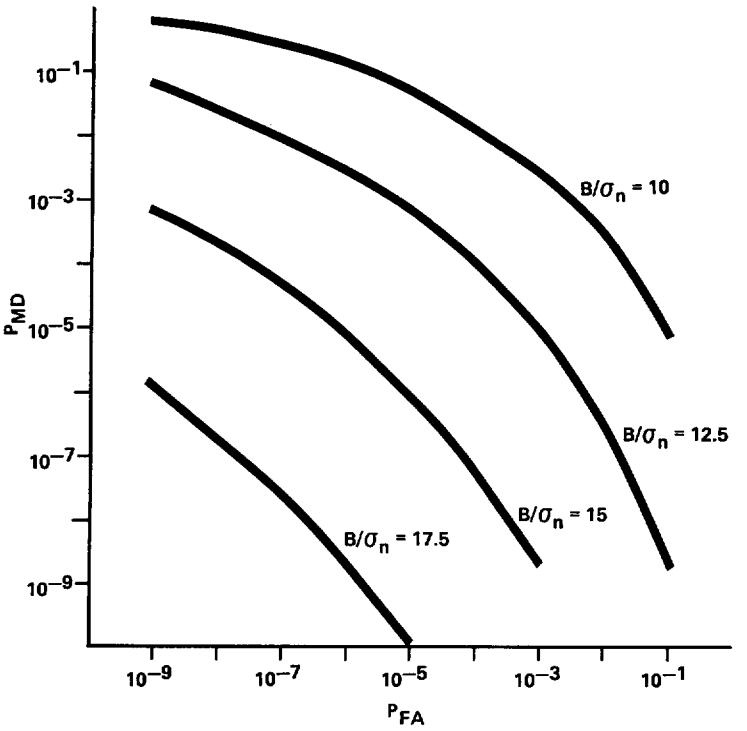

Fig. 3—DOCs for Five Sensors Equally Spaced on a Cone

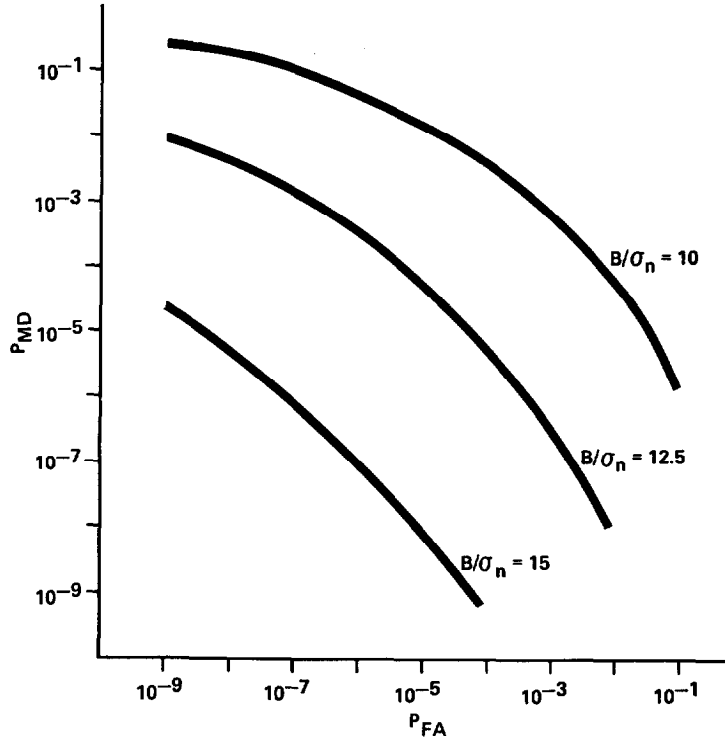

Fig. 4—DOCs for Six Sensors Equally Spaced on a Cone

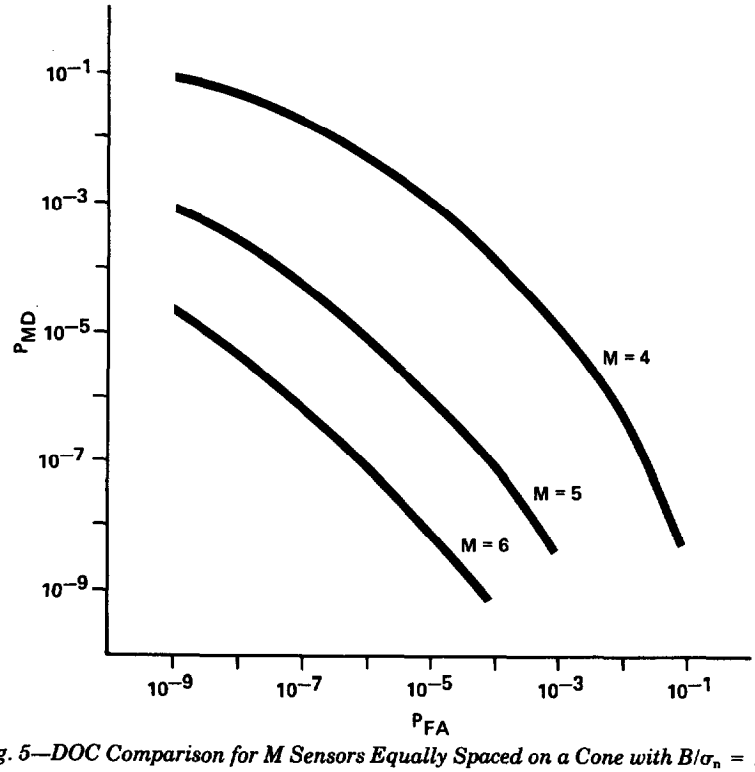

Fig. 5—DOC Comparison for M Sensors Equally Spaced on a Cone with $B/\sigma_n = 15$

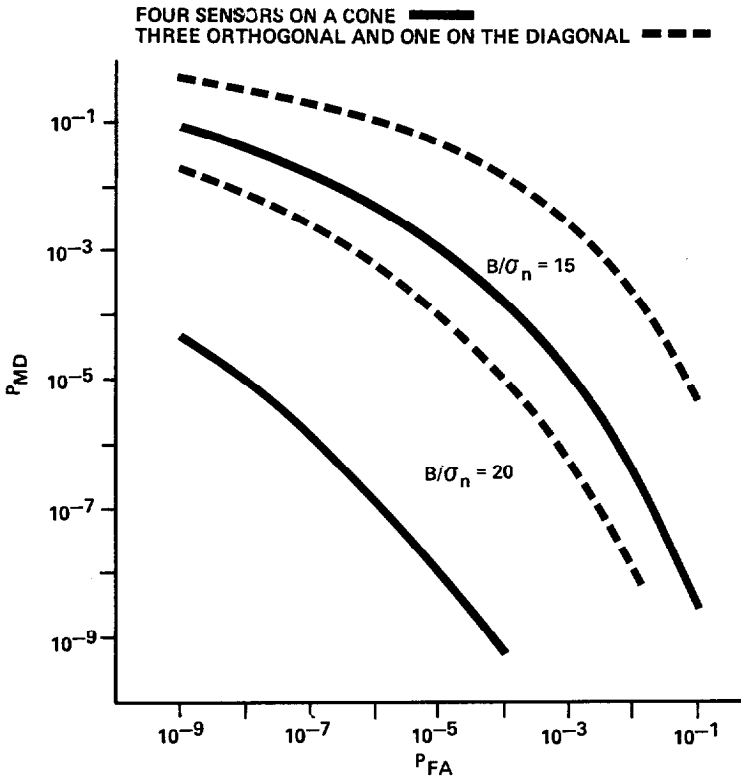

Fig. 6—Comparison of Four Sensor Configurations

$$V\ (\text{ft/sec}) = 101.1\ B_G(\text{deg/h})\ [1 - \cos(\omega_s t)]$$

and

$$V\ (\text{ft/sec}) = 25.9\ B_A(\text{mg})\ \sin(\omega_s t)$$

where ω_s is the Schuler frequency.

Thus a peak velocity of 8.4 ft/s is equivalent to a gyro bias shift of B_G = 0.042 deg/h or an accelerometer bias shift of B_A = 320 μg. The effects of instrument white noise and biases on T second Δθs and ΔVs are given by:

$$B_{\Delta\theta} = T\,B_G \qquad B_{\Delta V} = T\,B_A$$

$$\sigma_{\Delta\theta} = \sqrt{T}\,W_G \qquad \sigma_{\Delta V} = \sqrt{T}\,W_A.$$

Use of 10 s Δθs and ΔVs provides warning within 10 s of a fault occurring. The noises for 10 s samples are $\sigma_{\Delta\theta}$ = 0.028 arcsec and $\sigma_{\Delta V}$ = 0.0070 ft/s. The biases for 10 s samples are $B_{\Delta\theta}$ = 0.42 arcsec and $B_{\Delta V}$ = 0.10 ft/s. The resulting bias-to-standard deviation ratios are $B_{\Delta\theta}/\sigma_{\Delta\theta}$ = 15 and $B_{\Delta V}/\sigma_{\Delta V}$ = 15. Assuming a probability of false alarm of 10^{-6} (one false alarm every 0.3 operating years), the required thresholds are as follows:

Number of Sensors (M)	Δθ Threshold	ΔV Threshold
4	$(0.137\ \text{arcsec})^2$	$(0.034\ \text{ft/s})^2$
5	$(0.147\ \text{arcsec})^2$	$(0.037\ \text{ft/s})^2$
6	$(0.155\ \text{arcsec})^2$	$(0.039\ \text{ft/s})^2$

The probabilities of missed detection for both gyro and accelerometer faults are equal:

Number of Sensors (M)	P_{MD}	Number of Missed Detections per Million Faults
4	5×10^{-3}	5000
5	8×10^{-6}	8
6	1×10^{-7}	<1

GPS Navigation Set

The baseline 18-satellite GPS constellation is considered. This constellation consists of 6 orbital planes inclined 55 deg to the equator. Each plane contains 3 equally spaced satellites. The relative satellite phasing between planes is 40 deg. Three active spares ensure that at least 18 satellites are available 98 percent of the time. With an antenna mask angle of 5 deg, 5 or more satellites are visible 99.3 percent of the time. Instances of constellation deficiency (PDOP > 6) are ignored; they occur 0.5 percent of the time. The S matrix diagonal elements for this constellation vary considerably as a function of time and position. Their distribution is shown in Figure 7 for 5, 6, and 7 visible satellites.

The present integrity requirement for nonprecision approach is to detect a radial position error (RPE) of 0.3 nmi (550 m) within 10 s [9]. The equivalent $\widetilde{PR}$ bias shift is a function of the satellite geometry

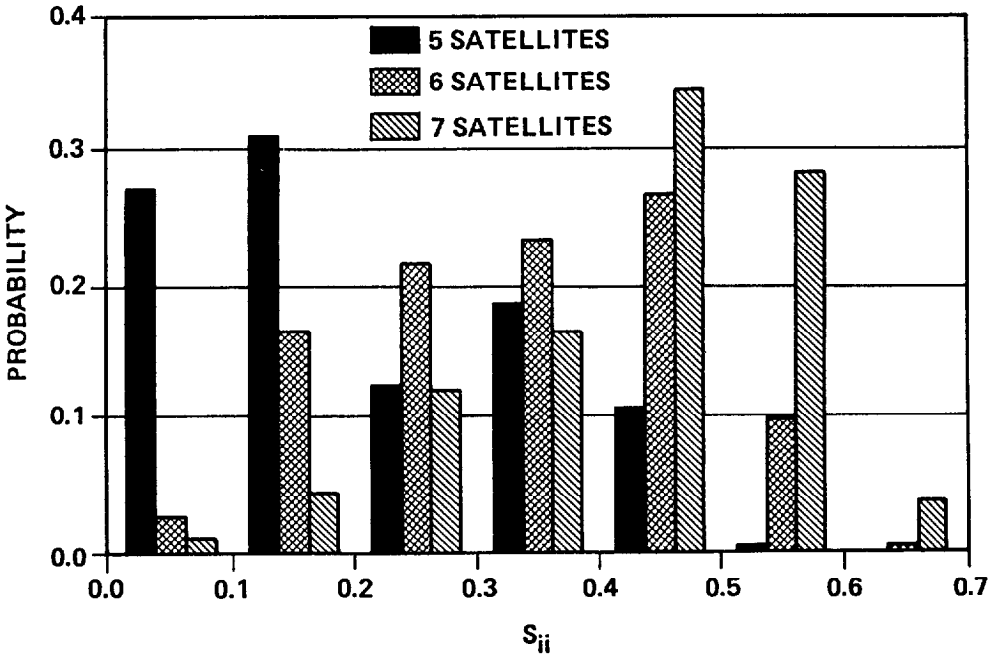

Fig. 7—Distribution of S_{ii}

$$B = \frac{RPE}{\sqrt{H^*_{1i}{}^2 + H^*_{2i}{}^2}} \tag{11}$$

where H^*_{1i} and H^*_{2i} are the elements of $\mathbf{H}^*$ that transform a bias in satellite i's PR measurement into the horizontal components of $\mathbf{x}$.

The noncentrality parameter in the DOC equation, equation (10), can be rewritten to group the geometry-dependent factors

$$\frac{B^2}{\sigma_n{}^2} S_{ii} = \left(\frac{S_{ii}}{H^*_{1i}{}^2 + H^*_{2i}{}^2}\right) \frac{RPE^2}{\sigma_n{}^2} . \tag{12}$$

Then equation (10) becomes

$$P_{MD} = \sum P\left(\frac{S_{ii}}{H^*_{1i}{}^2 + H^*_{2i}{}^2}\right) \times P\left(Q^{-1}(P_{FA}|M - N)|M - N, \left(\frac{S_{ii}}{H^*_{1i}{}^2 + H^*_{2i}{}^2}\right) \frac{RPE^2}{\sigma_n{}^2}\right) \tag{13}$$

where $P\,(S_{ii}/[H^*_{1i}{}^2 + H^*_{2i}{}^2])$ is the probability distribution of $S_{ii}/[H^*_{1i}{}^2 + H^*_{2i}{}^2]$, and the summation is over the distribution. This distribution is shown in Figure 8 for 5, 6, and 7 visible satellites. A second type of constellation deficiency is defined as instances when $S_{ii}/[H^*_{1i}{}^2 + H^*_{2i}{}^2] < 0.05$. These instances are ignored; they occur 6.8 percent of the time, almost exclusively when only 5 satellites are visible.

The GPS Standard Positioning Service provides a horizontal position accuracy of 100 m, 2 dRMS. The associated PR noise budget is [10]:

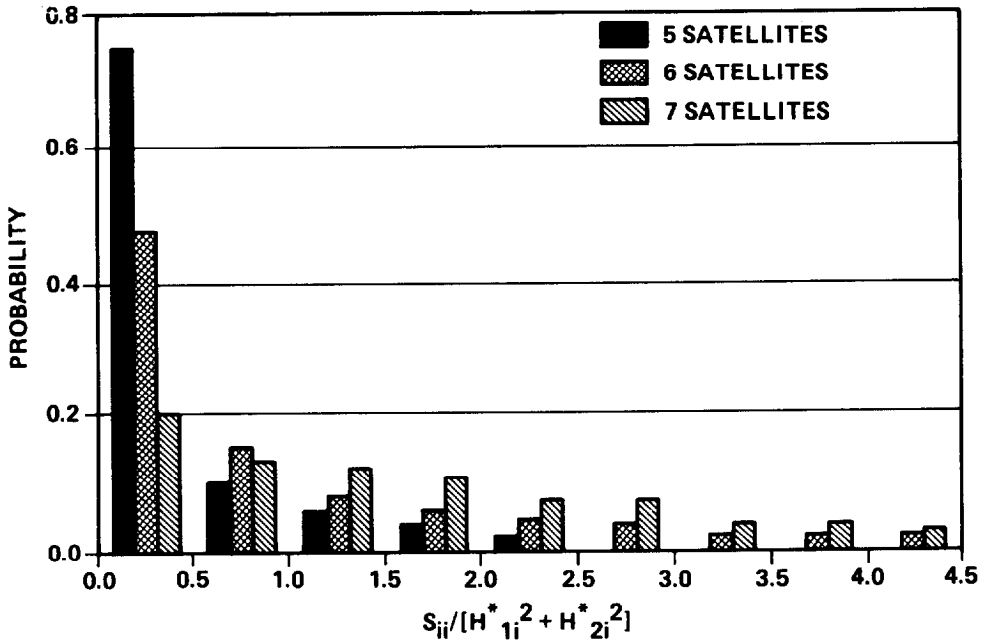

Fig. 8—Distribution of $S_{ii}/[H^*_{1i}{}^2 + H^*_{2i}{}^2]$

Noise Source	Standard Deviation	Noise Type
Satellite Clock and Ephemeris	5 m	Colored
Propagation Uncertainties	10 m	Colored
Receiver Noise	15 m	White
Selective Availability	30 m	Colored

The correlation times of the colored noise sources are modeled as significantly greater than 10 s. The $\widetilde{PR}$ standard deviation for a single measurement is the RSS of the individual noise sources. For a T second $\widetilde{PR}$ formed by averaging $\widetilde{PR}$ measurements made every 1 s over a T second interval, the contribution of the white noise sources is reduced by $1/\sqrt{T}$. Thus the 10 s average $\widetilde{PR}$ standard deviation is 32.4 m.

The radial position error-to-standard deviation ratio is $RPE/\sigma_n = 17.0$. DOCs for 5, 6, and 7 visible satellites are shown in Figure 9. Assuming a probability of false alarm of 10^{-6} (one false alarm every 0.3 operating year), the required thresholds are as follows:

Number of Visible Satellites (M)	$\widetilde{PR}$ Threshold
5	$(158\ m)^2$
6	$(170\ m)^2$
7	$(179\ m)^2$

A fault is declared if the square of the magnitude of the $\widetilde{PR}$ parity vector exceeds this value. The probabilities of missed detection are as follows:

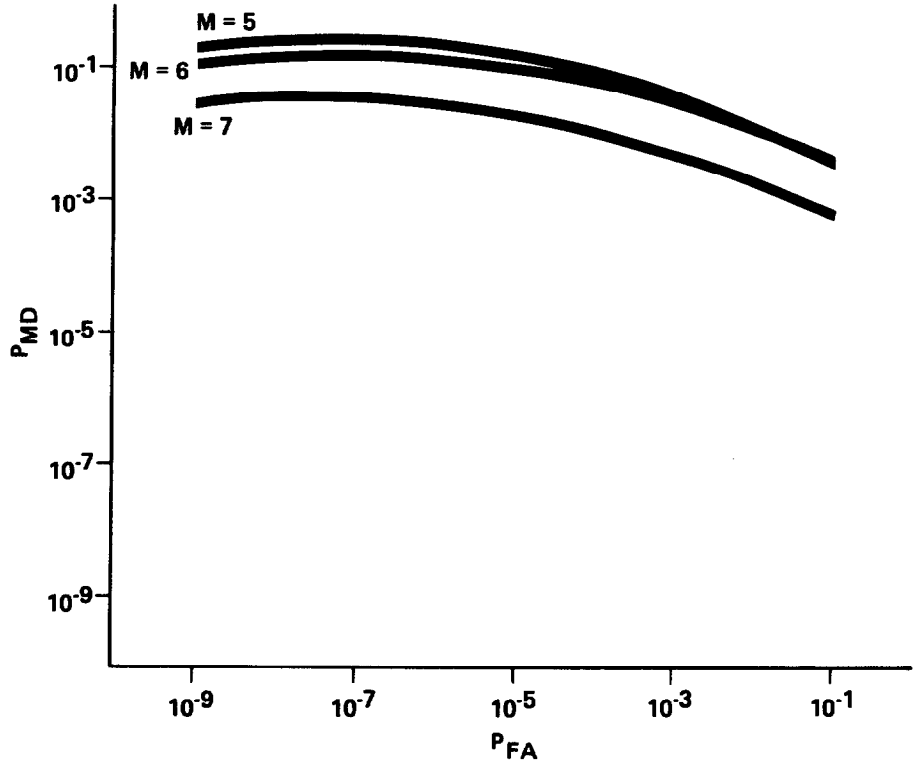

Fig. 9—DOCs for Five, Six, and Seven Visible Satellites with Selective Availability

Number of Visible Satellites (M)	P_{MD}	Number of Missed Detections per Million Faults
5	2×10^{-1}	200,000
6	1×10^{-1}	100,000
7	2×10^{-2}	20,000

This is obviously unacceptable performance.

Without Selective Availability (SA) noise, the 10 s average $\widetilde{PR}$ standard deviation is 12.1 m. The radial position error-to-standard deviation ratio is $RPE/\sigma_n = 45.5$. DOCs for 5, 6, and 7 visible satellite are shown in Figure 10. Assuming a probability of false alarm of 10^{-6}, the required thresholds are as follows:

Number of Visible Satellites (M)	$\widetilde{PR}$ Threshold
5	$(59 \text{ m})^2$
6	$(64 \text{ m})^2$
7	$(67 \text{ m})^2$

The probabilities of missed detections are as follows:

Number of Visible Satellites (M)	P_{MD}	Number of Missed Detections per Million Faults
5	1×10^{-8}	<<1
6	3×10^{-8}	<<1
7	6×10^{-9}	<<1

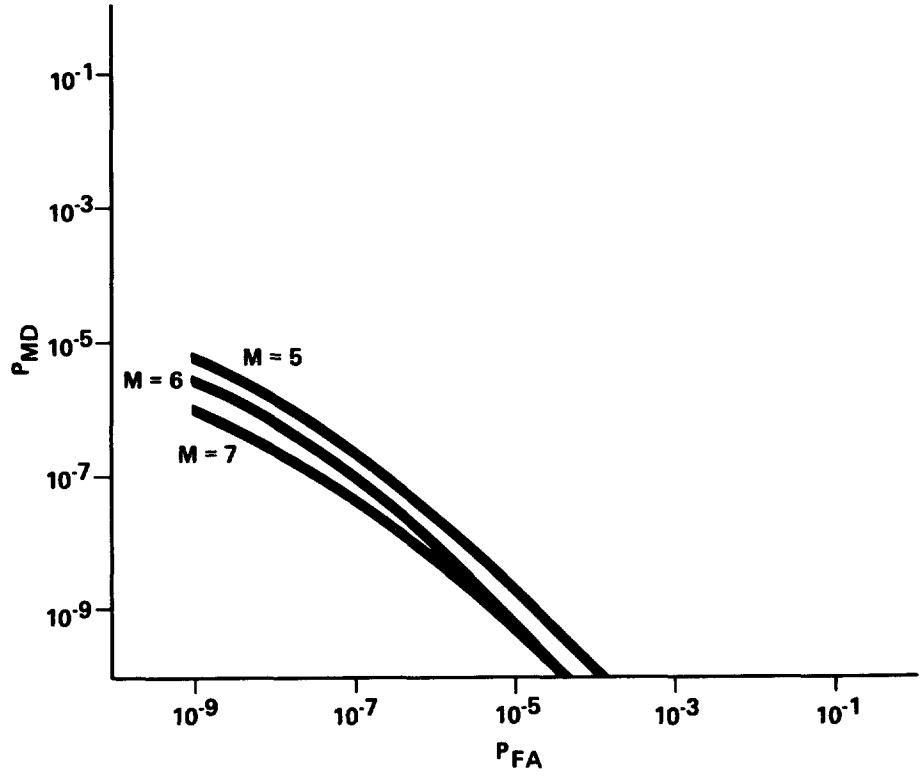

Fig. 10—DOCs for Five, Six, and Seven Visible Satellites without Selective Availability

This is excellent performance.

Figure 11 compares DOCs for 6 visible satellites with full SA noise, 1/2 SA noise, 1/3 SA noise, and no SA noise. As expected, the performance improves significantly as the SA noise is reduced.

FAULT IDENTIFICATION

If two or more redundant measurement sources are available, the faulty measurement source can potentially be identified. The maximum likelihood estimation (MLE) approach [12] to fault identification is to identify measurement source i as faulty if

$$P(\mathbf{p}|\mathbf{b}_i) = \underset{j}{\text{MAX}} \left\{ P(\mathbf{p}|\mathbf{b}_j) \right\}.$$

It is shown in Appendix C that the i that maximizes $P(\mathbf{p}|\mathbf{b}_i)$ also maximizes f_i^2/S_{ii}. Thus the MLE fault identification algorithm is as follows:

1) Compute the matrix $\mathbf{S} = \mathbf{I}_M - \mathbf{HH}^*$.
2) Compute the fault vector, $\mathbf{f} = \mathbf{Sz}$.
3) Compute the quantities f_i^2/S_{ii} for i = 1, ..., M.
4) Find the maximum f_i^2/S_{ii}. Then the measurement source i corresponding to the maximum value is identified as faulty.

The probability of misidentification, assuming that the measurement faults are equally likely, is

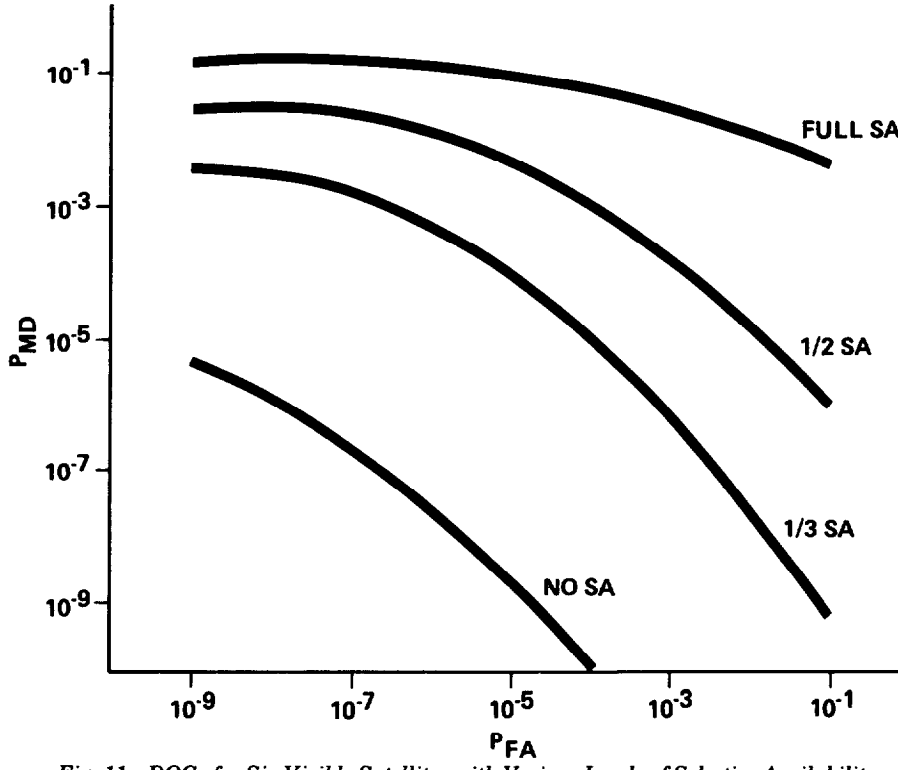

Fig. 11—DOCs for Six Visible Satellites with Various Levels of Selective Availability

$$P_{MI} = \frac{1}{M}\sum_{i=1}^{M} P\left[\frac{f_i^2}{S_{ii}} < \underset{j}{MAX}\left\{\frac{f_j^2}{S_{jj}}\right\} \middle| b_i\right]$$

CONCLUSION

In this paper, a measurement fault detection algorithm based on hypothesis testing has been described. The decision variable was the square of the magnitude of the parity vector. The test threshold was shown to be a function of the required P_{FA}, the number of redundant measurements, and the noise variance. The general form of the detector operating characteristic (DOC), characterizing the hypothesis test, was derived. The DOC was shown to be a function of the number of redundant measurements, the diagonals of the S matrix, and the ratio of the detectable bias shift to the noise variance.

DOCs for the configurations of four, five, and six sensors on a cone skewed axis inertial sensor were presented. For fixed bias-to-noise ratio (B/σ_n), the fault detection performance was shown to improve significantly as the number of sensors increased. The configuration of four sensors equally spaced on a cone was shown to have superior fault detection performance when compared to the configuration of three orthogonal sensors and one sensor on the diagonal.

GPS self-integrity monitoring for meeting nonprecision approach requirements (detecting a 550 m radial position error [RPE] within 10 s) was shown to be implausible in the presence of Selective Availability (SA) noise. This result was based on modeling the SA noise as colored, with a correlation time significantly greater than 10 s and a standard deviation of 30 m. Without SA noise, GPS self-integrity monitoring was shown to be possible.

A maximum likelihood estimation (MLE) fault identification algorithm was presented.

APPENDIX A
DIRECT COMPUTATION OF S MATRIX

Theorem: $\mathbf{S} = \mathbf{I}_M - \mathbf{H}\mathbf{H}^*$

Proof: That $\mathbf{A}^{-1} = [\mathbf{H}|\mathbf{P}^T]$ is the right inverse of

$$\mathbf{A} = \begin{bmatrix} \mathbf{H}^* \\ \cdots\cdots \\ \mathbf{P} \end{bmatrix}$$

is verified by direct multiplication:

$$\begin{aligned} \mathbf{A}\mathbf{A}^{-1} &= \begin{bmatrix} \mathbf{H}^* \\ \cdots\cdots \\ \mathbf{P} \end{bmatrix} [\mathbf{H}|\mathbf{P}^T] \\ &= \begin{bmatrix} \mathbf{H}^*\mathbf{H} & \mathbf{H}^*\mathbf{P}^T \\ \mathbf{P}\mathbf{H} & \mathbf{P}\mathbf{P}^T \end{bmatrix} \\ &= \begin{bmatrix} \mathbf{I}_N & \mathbf{O} \\ \mathbf{O} & \mathbf{I}_{M-N} \end{bmatrix} \\ &= \mathbf{I}_M \end{aligned}$$

Since A is square and of full rank, its left inverse must equal its right inverse. Thus

$$\begin{aligned} \mathbf{I}_M &= \mathbf{A}^{-1}\mathbf{A} \\ &= [\mathbf{H}|\mathbf{P}^T]\begin{bmatrix} \mathbf{H}^* \\ \cdots\cdots \\ \mathbf{P} \end{bmatrix} \\ &= \mathbf{H}\mathbf{H}^* + \mathbf{P}^T\mathbf{P} \\ &= \mathbf{H}\mathbf{H}^* + \mathbf{S}. \end{aligned}$$

Hence

$$\mathbf{S} = \mathbf{I}_M - \mathbf{H}\mathbf{H}^*.$$

Q.E.D.

APPENDIX B
CALCULATION OF DOCs

The DOCs presented in this paper were calculated from equation (10) using a variety of analytical and numerical techniques. The chi-square probability function, equation (6), was evaluated using the recursion

$$F(r, x) = -2x^{\frac{r}{2}-1}e^{-\frac{x}{2}} + 2\left(\frac{r}{2} - 1\right)F(r-2, x)$$

where

$$F(r, x) = \int_0^x t^{\frac{r}{2}-1}e^{-\frac{t}{2}}\,dt.$$

For $r = 2$,

$$F(r, x) = 2(1-e^{-x/2})$$

For $r = 1$, the integral was evaluated numerically by repeated application of the 5-point closed Newton-Cotes integration formulae. The integration step size was halved until successive evaluations differed by less than 10^{-12}.

The threshold-to-noise variance ratio, $K = T/\sigma_n^2$, was calculated by iteratively applying Newton's method to the equation

$$f(K) = 1 - P_{FA} - P(K, r) = 0.$$

The required derivative with respect to K is

$$f'(K) = -\left[2^{r/2}\,\Gamma\left(\frac{r}{2}\right)\right]^{-1} K^{\frac{r}{2}-1}e^{-K/2}.$$

The iterations were continued until f(K) was less than 10^{-12}.

The infinite sum in equation (10) was evaluated until $j! > 10^{12} * (\theta/2)^j$. All of the calculations were performed in double precision arithmetic (16 significant digits). The average computation time for each DOC on a PC-AT compatible computer at 8 MHz with an 80287 was 3 min for odd degrees of freedom and 15 s for even degrees of freedom.

APPENDIX C
MAXIMIZATION OF CONDITIONAL PROBABILITY

The parity vector has multivariate normal density with mean $\mathbf{Pb}$ and covariance $\sigma_n^2 \mathbf{I}_{M-N}$. Thus

$$P(\mathbf{p}|\mathbf{b}_i) = \frac{1}{(2\pi\sigma_n^2)^{\frac{M-N}{2}}} \exp\left[-\frac{1}{2\sigma_n^2}(\mathbf{p}-\mathbf{Pb}_i)^T(\mathbf{p}-\mathbf{Pb}_i)\right].$$

The i that maximizes $P(\mathbf{p}|\mathbf{b}_i)$ will maximize

$$-(\mathbf{p}-\mathbf{Pb}_i)^T(\mathbf{p}-\mathbf{Pb}_i)$$
$$= -\mathbf{p}^T\mathbf{p} + 2\mathbf{b}_i^T\mathbf{P}^T\mathbf{p} - \mathbf{b}_i^T\mathbf{P}^T\mathbf{Pb}_i.$$

Since $-\mathbf{p}^T\mathbf{p}$ is independent of i, it can be dropped. Taking advantage of the structure of $\mathbf{b}_i$, and the fact that $\mathbf{p} = \mathbf{Pz}$, this reduces to

$$2B\mathbf{S}_i\mathbf{z} - B^2S_{ii}$$

where $\mathbf{S}_i$ is the ith row of $\mathbf{S}$. The value of B that maximizes this quantity is obtained by setting its derivative with respect to B to zero. This gives

$$\hat{B} = \frac{\mathbf{S}_i\mathbf{z}}{S_{ii}}.$$

Back substituting and noting that $f_i = \mathbf{S}_i\mathbf{z}$ gives f_i^2/S_{ii}.

Thus maximizing f_i^2/S_{ii} is equivalent to maximizing $P(\mathbf{p}|\mathbf{b}_i)$.

Based on a paper presented at the Institute of Navigation's National Technical Meeting, Santa Barbara, CA, January 1988.

REFERENCES

1. *1986 Federal Radionavigation Plan,* DOD-4650. 4, DOT-TSC-RSPA-87-3.
2. Pejsa, A. J., *Optimum Orientation and Accuracy of Redundant Sensor Arrays,* AIAA 9th Aerospace Sciences Meeting, January 1971.
3. Bejczy, A. K., *Non-orthogonal Redundant Configurations of Single-Axis Strapped-Down Gyros,* JPL Quarterly Technical Review, Vol. 1, No. 2, July 1971, pp. 107–118.
4. Sebring, D. L. and Young, J. T., *Redundancy Management of Skewed and Dispersed Inertial Sensors,* 4th DASC, November 1981, pp. 383–391.
5. Ephgrave, J. T., *Optimum Redundant Configurations of Inertial Sensors,* Aerospace Corporation, AD-749 561, September 1966.
6. Wei, S. Y. and Huddle, J. R., *Sensor Management for a Fault Tolerant Integrated Inertial Flight Control Reference and Navigation System,* IEEE PLANS '86, November 1986, pp. 445– 455.
7. Gai, E., Harrison, J. V., and Daly, K. C., *FDI Performance of Two Redundant Sensor Configurations,* IEEE Transactions, Vol. AES-15, No. 3, May 1979, pp. 405–413.
8. Jeerage, M. and Boettcher, K., *Fault Tolerant Highly Reliable Inertial Navigation System,* IEEE PLANS '86, November 1986, pp. 456–460.
9. *Report of the SC-159 Integrity Working Group,* RTCA paper no. 220-87/SC 159-95, May 6, 1987.
10. Brown, A. K., *Civil Aviation Integrity Requirements for the Global Positioning System,* NAVIGATION, Journal of The Institute of Navigation, Vol. 35, No. 1, Spring 1988, pp. 23–40.
11. Parkinson, B. W. and Axelrad, P., *Autonomous GPS Integrity Monitoring Using the Pseudorange Residual,* NAVIGATION, Journal of The Institute of Navigation, Vol. 35, No. 2, Summer 1988, pp. 255–274.
12. Duda, R. O. and Hart, E. H., *Pattern Clarification and Scene Analysis,* New York: John Wiley & Sons, Inc., 1973, Chapters 2 and 3.